Analytical Methods

Effective Discrimination of Gas-Phase Peptide Conformers using TIMS-ECD-ToF MS/MS

Journal:	*Analytical Methods*
Manuscript ID	AY-ART-08-2021-001461.R1
Article Type:	Paper
Date Submitted by the Author:	08-Oct-2021
Complete List of Authors:	Jeanne dit fouque, Kevin ; Florida International University, Chemistry and Biochemistry Wellmann, Malte ; Florida International University, Chemistry and Biochemistry Leyva , Dennys; Florida International University, Chemistry and Biochemistry Santos-Fernandez, Miguel ; Florida International University, Chemistry and Biochemistry Cintron Diaz , Yarixa ; Florida International University, Chemistry and Biochemistry Gomez-Hernandez, Mario ; Florida International University, Chemistry and Biochemistry Kaplan, Desmond; 2KapScience LLC Voinov, Valery; e-MSion Inc. Fernandez-Lima, Francisco; Florida International University, Chemistry and Biochemistry

Analytical Methods

ARTICLE

Effective Discrimination of Gas-Phase Peptide Conformers using TIMS-ECD-ToF MS/MS

Received 00th January 20xx,
Accepted 00th January 20xx

DOI: 10.1039/x0xx00000x

www.rsc.org/

K. Jeanne Dit Fouque,[a,b] M. Wellmann,[c] D. Leyva Bombuse,[a] M. Santos-Fernandez,[a] Y. L. Cintron-Diaz,[a] M. E. Gomez-Hernandez,[a] D. Kaplan,[d] V. G. Voinov,[e,f] and F. Fernandez-Lima*[a,b]

In the present work, four, well-studied, model peptides (e.g., substance P, bradykinin, angiotensin I and AT-Hook 3) were used to correlate structural information provided by ion mobility and ECD/CID fragmentation in a TIMS-q-EMS-ToF MS/MS platform, incorporporating an electromagnetostatic cell (EMS). The structural heterogeneity of the model peptides was observed by i) multi-component ion mobility profiles (high ion mobility resolving power, R ~ 115-145), and ii) fast online characteristic ECD fragmentation patterns per ion mobility band (~ 0.2 min). Particularly, it was demonstrated that all investigated species were probably conformers, involving *cis*/*trans*-isomerizations at X-Pro peptide bond, following the same protonation schemes, in good agreement with previous ion mobility and single point mutation experiments. The comparison between ion mobility selected ECD spectra and traditional FT-ICR ECD MS/MS spectra showed comparable ECD fragmentation efficiencies but differences in the ratio of radical (•)/prime (') fragment species (H• transfer), which were associated with the differences in detection time after the electron capture event. The analysis of model peptides using online TIMS-q-EMSToF MS/MS provided complementary structural information on the intramolecular interactions that stabilize the different gas-phase conformations to those obtained by ion mobility or ECD alone.

Introduction

Electron capture/transfer dissociation (ECD/ETD) are widely used low energy, electron-based fragmentation techniques for the structural elucidation of peptides and proteins in tandem mass spectrometry (MS/MS).[1-3] Advances in electron-based fragmentation (ExD) approaches have significantly improved middle-down and top-down proteomics by providing complementary structural information and increasing the sequence coverage.[2-5] In particular, ExD methods afford several advantages over traditional slow-heating activation techniques (e.g., collision induced dissociation, CID, and infrared multiple photon dissociation, IRMPD). ECD/ETD reactions primarily cleave the strongest peptide backbone N–Cα as well as disulfide bonds,[6, 7] while conserving the weakest C-N peptide bonds.[1-3] This process generates complementary even-electron c_i' and odd-electron $z_j^{\bullet}$ product ions arising from the dissociation of the charge-reduced $[M + zH]^{(z-1)\bullet}$ species. Moreover, ExD techniques preserve the labile post-translational modifications (PTMs), such as glycosylation, phosphorylation and others.[8-13] Non-covalent interactions can also be conserved in ExD, enabling the identification of protein-ligand binding sites by top-down mass spectrometry.[14-17] One limitation to ExD is related to proline residues, for which cleavages are rarely occurring due to its cyclic secondary amine structure.[1-3] Note that ExD methods require multiply charged precursor ions to produce the charge-reduced species, making these techniques very well-suited with electrospray ionization (ESI).

Since the introduction of ECD[18, 19] and ETD,[20, 21] several studies have been focused on the ion-electron specificity and mechanism for cleaving the peptide backbone N–Cα bond. The ergodicity or non-ergodicity mechanism of ECD is still hotly debated.[22, 23] McLafferty and co-workers proposed the Cornell mechanism (Scheme S1a),[18] where electron attachment occurs in a Rydberg orbital at a basic site (e.g., N-terminus, Arg, Lys or His residues) leading to a hypervalent radical species. The nature of this orbital combined with the excess energy supplied by the electron (4 to 6 eV) allow to reach relaxation processes that result in H transfer leading to the cleavage of the peptide backbone N–Cα bond (Scheme S1a). Simons and co-workers[24] as well as Turecek and co-workers[25] proposed the Utah–

[a] Department of Chemistry and Biochemistry, Florida International University, Miami, FL 33199, United States.
E-mail: fernandf@fiu.edu
[b] Biomolecular Science Institute, Florida International University, Miami, FL 33199, United States.
[c] Institute of Physical Chemistry, Christian-Albrechts-University Kiel, 24098 Kiel, Germany.
[d] KapScience LLC, Tewksbury, MA 01876, United States.
[e] e-MSion Inc., Corvallis, OR 97330, United States.
[f] Linus Pauling Institute and Department of Biochemistry and Biophysics, Oregon State University, Corvallis, OR 97331, United States.
† Electronic Supplementary Information (ESI) available: Schematics showing the Cornell and Utah–Washington mechanisms for N–Cα bond cleavage in ExD and TIMS-q-EMS-CC-oToF MS instrument, Optimized settings in the transmission and ECD modes for the EMS cell, ECD/CID spectra of the selected $[M + 2H]^{2+}$ ions of substance P, angiotensin I, bradykinin and AT-Hook 3 acquired in TIMS-q-ECD-ToF MS and FT-ICR MS platforms and ECD efficiency yields of the investigated peptides. DOI: 10.1039/x0xx00000x

Washington mechanism (Scheme S1b), for which electron attachment occurs in a π* antibonding orbital of the amide group, generating an aminoketyl radical anion. These labile radical species are then dissociated by N–Cα bond cleavage, resulting from a proton transfer from a charged site (Scheme S1b). Several other ExD mechanisms based on the Cornell and Utah–Washington proposals have been also suggested over the years.[26-30] One specificity of ExD methods is the formation of odd-electron $c_i^{\bullet}$ and even-electron z_j' product ions in addition to regular c_i' and $z_j^{\bullet}$ fragment species via H• migration (Figure 1a).[31] This feature has been proposed to take place within long-lived $[c_i' + z_j^{\bullet}]$ ion–dipole or ion–ion complexes before breaking apart.[32, 33] In fact, if the lifetime of the $[c_i' + z_j^{\bullet}]$ complex is long enough, an H• transfer may occur, resulting in the formation of $c_i^{\bullet}$ ($c_i^{\bullet} = c_i' - H$) and z_j' ($z_j' = z_j^{\bullet} + H$) product ions as illustrated in Figure 1b. In addition, several studies reported that the lifetime of the $[c_i' + z_j^{\bullet}]$ complex is strongly influenced by the gas-phase conformation.[34-36]

Generally, ETD is more employed than ECD for the structural analysis of peptides and proteins due to its efficient implementation on relatively affordable ion trap and hybrid q-ToF mass spectrometers, as compared to FT-ICR MS instruments. In 2008, Barofsky and co-workers introduced an electromagnetostatic (EMS) cell, capable of performing ECD without the need for long reaction times or ultrahigh vacuum.[37, 38] In addition, the EMS cell was successfully retrofitted into widespread triple quadrupole,[39-41] q-ToF[42-44] and Orbitrap[45-48] mass spectrometers. Several reports have shown the advantages of ExD in combination with ion mobility spectrometry (IMS) for full characterization of isomeric species.[49-53] The EMS cell has been recently coupled to a q-TWIMS-EMS-ToF[44] (Synapt G2-S*i*) and a DTIMS-q-EMS-ToF[54] (Agilent 6560) MS/MS platforms. A novel TIMS-q-EMS-ToF MS/MS instrument was recently utilized for the separation of histone tail proteoforms with known PTM locations from binary isomeric and isobaric mixtures.[55] The TIMS-q-EMS-ToF MS/MS platform comprises a new EMS cell design (~2x shorter), utilizes Ar instead of N_2 in the collision cell, and provides superior ion mobility separation when compared to the other two aforementioned implementations (i.e., 2x-3x higher ion mobility resolving power).

In the present work, we report on the analysis of doubly protonated model peptides (e.g., substance P, bradykinin, angiotensin I and AT-Hook 3) using the novel TIMS-q-EMS-ToF MS/MS platform. Two fundamental questions are addressed: i) Can ion mobility-selected ECD provide fingerprints associated with the gas-phase conformational isomers?, and ii) Are there fundamental differences between the ECD observed in the EMS cell when compared to traditional ECD implemented in the FT-ICR-MS?. Differences between the ion mobility selected ECD spectra are discussed based on the type and relative intensity of the fragment ions (e.g., $[c_i' + z_j^{\bullet}]$ and $[c^{\bullet} + z_j']$ complex ions) and with traditional FT-ICR ECD-MS/MS. In the following discussion, a special emphasis is placed on the structural information provided by the ion mobility selected ECD spectra when compared with previously reported studies of these model peptide systems.

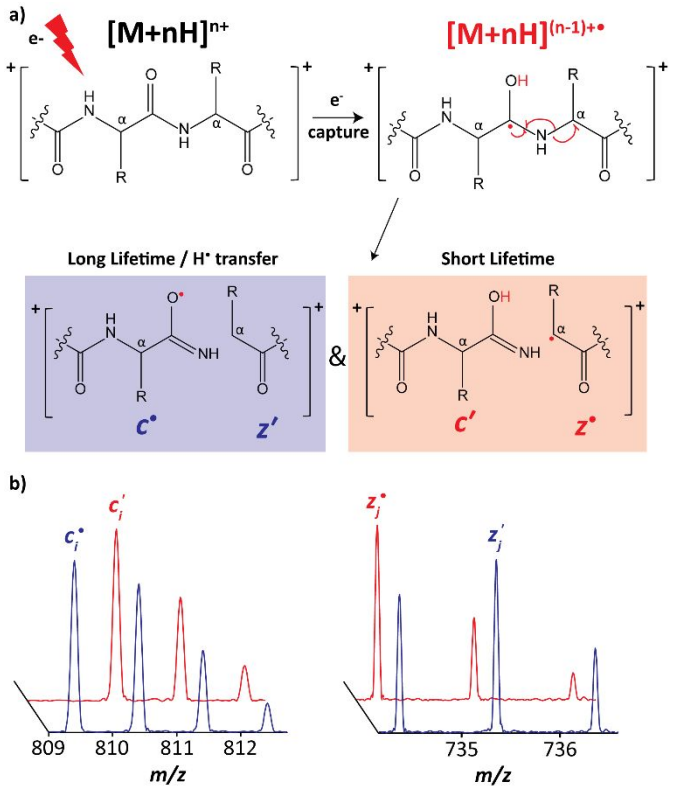

Figure 1. Illustration showing (a) the pathway of radical/even-electron pairs for c_i and z_j product ions in ExD and (b) typical isotopic distribution for classical short lifetime $[c_i' + z_j^{\bullet}]$ (red traces) and long lifetime $[c_i^{\bullet} + z_j']$ (blue traces) fragment species. Note that a slight offset of the isotopic distribution for classical short lifetime $[c_i' + z_j^{\bullet}]$ fragment species (red traces) was incremented for better visualization.

Experimental

Materials and Reagents

Angiotensin I (DRVYIHPFHL, 1296 Da), bradykinin (RPPGFSPFR, 1060 Da) and substance P (RPKPQQFFGLM, 1347 Da) were purchased from Sigma-Aldrich (Saint. Louis, MO). AT-Hook 3 (KRPRGRPRKW, 1338 Da) were obtained from GenScript (Piscataway, NJ). All peptide solutions were analyzed at a concentration of 5 µM in 50:50 water/methanol (H_2O/MeOH) solvent conditions with 0.1% formic acid (FA). A low concentration Tuning Mix standard (G1969-85000) was used for ion mobility and mass calibration purposes and obtained from Agilent Technologies (Santa Clara, CA).

TIMS-q-ECD/CID-ToF MS/MS Instrumentation

Ion mobility experiments were carried out on a custom built nanoESI-TIMS-q-EMS-ToF MS/MS (Bruker Daltonics Inc., Billerica, MA, Figure S1).[56, 57] The nanoESI emitters were pulled in-house from quartz capillaries (O.D. = 1.0 mm and I.D. = 0.70 mm) using a Sutter Instrument Co. P2000 laser puller. Peptide sample solutions were loaded in a pulled-tip capillary, housed in a mounted custom built XYZ stage in front of the MS inlet, and sprayed at ~700 V via a tungsten wire inserted inside the nanoESI emitters. The TIMS unit was controlled by an in-house software in LabView (National Instruments) and synchronized

with the ToF-MS platform controls.[57] The general fundamentals of TIMS as well as the calibration procedure have been previously described in the literature.[58-63] TIMS-MS experiments were performed using nitrogen (N_2) at ambient temperature (T) with a gas velocity (v_g) defined by the funnel entrance (P_1 = 2.6 mbar) and exit (P_2 = 0.8 mbar) pressure differences. An rf voltage of 250 Vpp at 880 kHz was applied to all electrodes. A deflector voltage (V_{def}) of 80 V, a base voltage (V_{out}) of 60 V voltage as well as a ramp voltage (V_{ramp}) of -120 to -90 V (Bradykinin), and -145 to -115 V (Angiotensin I, Substance P and AT-Hook 3) were used for the ion mobility separations. The scan rate ($Sr = \Delta V_{ramp}/t_{ramp}$) was optimized for fast TIMS-ToF MS acquisition while keeping a high ion mobility separation. All resolving power (R) values reported herein were determined as R = CCS/ΔCCS, where ΔCCS is the full peak width at half maximum (FWHM) of the IMS profile. The reported errors account for the variations observed in the triplicate measurements. The relative intensities for each replicate were determined using the peak heights of each fragment divided by the sum of all fragments for direct comparison across the IMS bands.

A new EMS (e-MSion Inc., Corvallis, OR) was attached to a custom-built collision cell and mounted between the quadrupole exit and the pulsing plates of the ToF MS instrument (Figure S1). The shortened collision cell was operated at 1800 Vpp and 2.3 MHz. The new EMS cell (19 mm long) is composed of seven cylindrical electrostatic lenses (L1-L7), two ring magnets and a heated rhenium filament (Scientific Instrument Services, Ringoes, NJ) housed in L4, where electrons are generated at the center of the cell (Figure S1). Electrons are confined along the ion longitudinal axis. The filament was operated at a current of 2.5 A. The electrostatic lenses applied to the EMS cell were tuned to get maximum ion intensity in the transmission mode (non-ECD mode) and optimal ECD fragmentation events in ECD mode (Table S1). No changes to the TIMS-TOF MS operation were required due to the fast speed of the ECD events (~ 10 µs),[38, 46] that is, ECD spectra were collected for each ion mobility scan step allowing for precursor-fragments ion mobility alignment. Collision-induced dissociation (CID) MS/MS experiments of the $[M+2H]^{2+}$ ions were performed with the EMS cell in transmission mode (filament off) in the shortened, custom built collision cell, filled with residual high purity argon (oxygen free) at 5E-4 mbar and a collision voltage of ~32 eV. During ECD only experiments, the collision voltage was set to 6 eV. All data corresponds to acquisitions of ~ 0.2 min.

FT-ICR MS Instrumentation

Complementary ECD experiments were conducted on a Solarix 7T FT-ICR mass spectrometer (Bruker, Billerica, MA) equipped with an Infinity cell and a nanoESI source operated in positive ion mode. Sample aliquots (10 µL of 3 µM solution) were loaded in a pulled-tip capillary mounted on a custom built XYZ stage in front of the MS capillary inlet. The high voltage, capillary exit, and skimmer I were set to 1400 V, 140 V, and 30 V respectively. Precursor ions were isolated in the quadrupole with a mass window of 5 Da, accumulated for 0.5 s in the collision cell, and further injected into the ICR cell. ECD experiments were performed with a heated hollow cathode operating at a current of 1.52 A. The ECD pulse length, ECD Bias and ECD Lens were set at 0.12 s, 1.2 V, and 10 V respectively. A total of 150 scans (m/z range 100-2000) were co-added with a data acquisition size of 512k words.

RESULTS AND DISCUSSION

TIMS-q-EMS-ToF MS/MS and FT-ICR ECD MS/MS experiments were carried out on the $[M + 2H]^{2+}$ ions of substance P, bradykinin, angiotensin I, and AT-Hook 3 peptides under the same denaturing conditions (e.g., 50:50 H_2O/MeOH, 0.1% FA).

Ion Mobility selected –ECD/CID MS/MS of Substance P $[M + 2H]^{2+}$

Typical ion mobility, precursor ion mass and relative intensity of observed ECD fragments in TIMS-q-EMS-ToF MS/MS and FT-ICR ECD MS/MS of the substance P $[M + 2H]^{2+}$ molecular ion are shown in Figure 2. The TIMS analysis resulted in the observation of two baseline separated IMS bands, with an apparent ion mobility R ~ 115 using a Sr = 0.26 V/ms (Figure 2a). Note that a much higher ion mobility separation is needed to separate these IMS bands, when compared with those observed for the $[M + 3H]^{3+}$.[64, 65] Inspection of the ion mobility-selected ECD/CID spectra showed similar features between the IMS 1 and IMS 2 bands as well as the FT-ICR ECD MS/MS spectra (Figure S2). In all TIMS-q-EMS-ToF MS/MS spectra, the charge-reduced $[M + 2H]^{\bullet+}$ ions (m/z 1347.7) were always observed, as signature ions of the ECD events. In addition, $c_i'/z_j^{\bullet}$ series were observed, consisting of c_2' to c_{10}' (except for c_3' due to Pro4) and $z_9^{\bullet}$ product ions (Figure 2c). Note that the lack of $z_j^{\bullet}$ series (only $z_9^{\bullet}$) is consistent with the presence of basic sites located near the N-terminus (Arg1 and Lys3) as well as Pro2 and Pro4 residues that prevent N–Cα bond cleavage. In the TIMS-q-EMS-ToF MS/MS experiments, a fragmentation efficiency of ~ 2% relative to the intensity of the precursor ions was obtained for the most abundant c_5' product ions. This ECD efficiency is slightly higher than those observed in previous implementations of the EMS cell (~ 1%).[41, 42] While the EMS operation was optimized mainly for ECD events, a small presence of CID-like events, involving b_i/y_j series ions, were observed consistent with previous EMS implementations.[38, 42] The observation of CID-like ions has been attributed to collisions with the residual gas (Ar instead of N_2 in our case) and potential precursor ion excitation during the quadrupole precursor isolation (m/z 10 Da window, Figure 2b). The b_i/y_j fragment ions enabled the cleavage at Pro residues, which allowed to obtain full sequence coverage when compared with sole ECD. The total ECD fragmentation efficiency obtained in the TIMS-q-EMS-ToF MS/MS platform matches that of the FT-ICR ECD MS/MS (~ 8% vs. ~ 7%, respectively, Table S2). Different extents of hydrogen migration (H• transfer) were observed between the two platforms (Figure 2d). While no significant H• transfer was observed in the EMS cell for the c_i' series, c_4' and c_5' fragments were partially shifted by 1 Da from

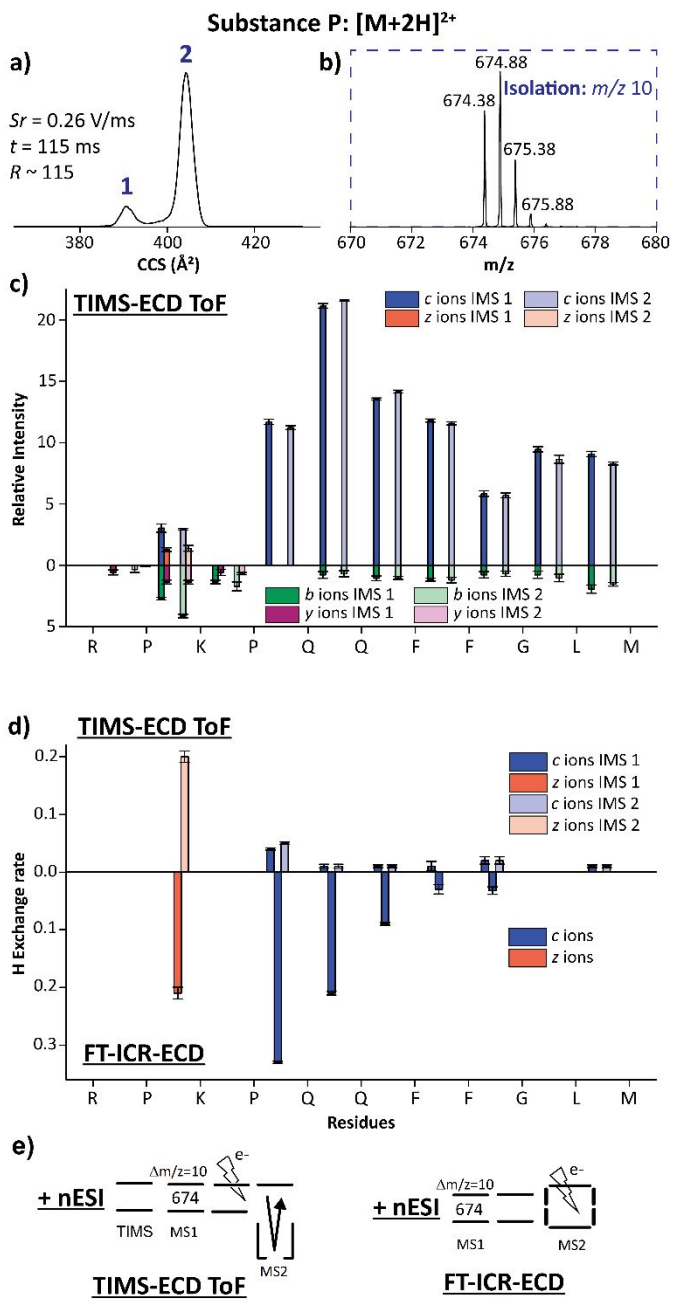

Figure 2. TIMS-q-EMS-ToF and FT-ICR-ECD MS/MS analysis of substance P $[M + 2H]^{2+}$ ions (*m/z* 674.4). (a) Typical TIMS profiles, (b) quadrupole isolation window of the precursor ion, (c) bar plots showing the relative intensities of the ECD product ions per IMS bands for the selected $[M + 2H]^{2+}$ ions, (d) bar plot showing the hydrogen migration events of substance P observed in the two MS platforms, obtained by comparison between the experimental and theoretical isotopic patterns, and e) representative schematics of the TIMS-ECD-TOF and FT-ICR ECD MS/MS experiments. Note that relative intensities were calculated using peak heights and divided by the sum of all fragments for direct comparison across IMS bands. c_i/z_j and b_i/y_j ions are plotted above and below the horizontal axis, respectively in (c). Error bars from triplicate measurements are represented on the bar plots. Ion mobility selected ECD/CID and FT-ICR ECD spectra are shown in Figure S2).

a loss of H•, giving the $c_4^{\bullet}$ and $c_5^{\bullet}$ product ions in the FT-ICR MS. In addition, $z_9^{\bullet}$ fragments appeared to be shifted by the capture of H•, giving the z_9' product ions in both platforms (Figure S2).

Intramolecular H• migration is strongly influenced by the gas-phase conformation,[7, 34-36] suggesting that a rigid fold may be induced by the two proline residues (Pro2 and Pro4). This fold may bring the Pro4 and Gln5 residues in proximity to each other and/or with other residues, facilitating H• transfer. The differences between TIMS-q-EMS-ToF MS and FT-ICR ECD MS/MS platforms in the ratio of radical (•)/prime (') fragment species can be associated with the differences in detection time after the electron capture event. For example, ions do not experience any collision prior to the ICR detection (hundreds of milliseconds) after the ECD event in the FT-ICR MS, while in the EMS cell, ions enter the collision cell (few milliseconds) prior to the TOF MS detection. $[c_i' + z_j^{\bullet}]$ complexes do not need much energy to be separated (hold by non-covalent bonds), so most of them dissociate almost immediately in the collision cell. This is also consistent with the observation of CID-like fragments in the ECD experiments, suggesting that there are collisions with the residual gas, leading to shorter lifetimes of the $[c_i' + z_j^{\bullet}]$ complex and then reducing the probability for H• transfer, in good agreement with previous observations.[33, 66]

Figures 2c and S2f display the relative intensity of each $c_i'/z_j^{\bullet}$ and b_i/y_j product ions per IMS bands. Overall, the fragmentation pattern in the $c_i'/z_j^{\bullet}$ and b_i/y_j fragments were similar for the two IMS bands, suggesting that these two structures are probably conformers that follow the same protonation scheme. In fact, the presence of $z_9^{\bullet}$ together with c_2' fragments for both IMS bands indicated that the Lys3 and Arg1 residues probably carry the charge. However, differences in the relative intensity and hydrogen exchange were observed at Pro2 residues. The relative intensity of the b_2 product ions was found higher in the IMS band 2 as compared to IMS band 1 (green bars in Figure 2c). This is consistent with a conformational change involving a *cis*/*trans*-isomerization at Arg1-Pro2 peptide bond, as previously described by Clemmer and co-workers.[67] Prolines in the *cis*-configuration require slightly higher energy to cleave the peptide bond than a proline in a *trans*-configuration. This result suggests that the most compact structure (IMS 1 band) involves an Arg1-Pro2 peptide bond in a *cis*-configuration, while the most extended structure (IMS 2 band) have the Pro2 in a *trans*-configuration. In addition, z_9' and $c_4^{\bullet}$ product ions exhibited different hydrogen exchange, for which higher abundance of H• migration was observed for IMS 2 band (Figure 2d). This suggests that the *trans*-configuration probably brings the Arg1-Gln5 residues in close proximity to each other, facilitating H• transfer (slower dissociation), while the *cis*-configuration might not be positioned in a way that allows H• transfer as frequently (faster dissociation). No differences were observed between the ion mobility-selected CID spectra (Figure S2); the fragmentation patterns do not retain any memory of the gas-phase molecular conformers.

Ion Mobility selected –ECD/CID MS/MS of AT-Hook 3 $[M + 2H]^{2+}$

Typical ion mobility, precursor ion mass and relative intensity of observed ECD fragments in TIMS-q-EMS-ToF MS/MS and FT-ICR ECD MS/MS of the $[M + 2H]^{2+}$ AT-Hook 3 molecular ion are shown in Figure 3. The TIMS analysis for the $[M + 2H]^{2+}$ molecular species of AT-Hook 3 resulted in the observation of

three relatively well-resolved IMS bands, separated with an apparent ion mobility R ~ 120 using a Sr = 0.26 V/ms (Figure 3a), in agreement with previous TIMS-ToF MS experiments.[68] Inspection of the ion mobility-selected ECD/CID spectra showed similar features between the IMS 1, IMS 2 and IMS 3 bands as well as the FT-ICR ECD MS/MS spectra (Figure S3). The charge-reduced $[M + 2H]^{\bullet+}$ ions (m/z 1337.8) were always observed, as signature ions of the ECD events. In addition, $c_i'/z_j^{\bullet}$ series were observed, consisting of c_4' to c_9' and $z_5^{\bullet}$ to $z_9^{\bullet}$ product ions (except for c_6' and $z_8^{\bullet}$ due to Pro7 and Pro3, respectively, Figure 3c). In the TIMS-q-EMS-ToF MS/MS experiments, a fragmentation efficiency of ~ 1% relative to the intensity of the precursor ions was observed for the most abundant c_8' ECD product ions. The total ECD fragmentation efficiency obtained in the TIMS-q-EMS-ToF MS/MS platform was lower than that of the FT-ICR ECD MS/MS (~ 5% vs. ~ 19%, respectively, Table S2), however, the hydrogen migration (H• transfer) were comparable between the two platforms (Figure 3d). Product ions that involve significant H• migration were mainly observed in the Lys1-Arg2 (z_9'), Arg4-Gly5 ($c_4^{\bullet}/z_6'$), Gly5-Arg6 ($c_5^{\bullet}/z_5'$), Pro7-Arg8 ($c_7^{\bullet}$) and Lys9-Trp10 ($c_9^{\bullet}$) N–Cα bonds. Interestingly, H• transfer events were observed across the entire sequence (except at Pro residues), suggesting that most of the residues are in proximity to nearby residues due to orientation of proline residues (Pro3 and Pro7) and/or via charge solvation, including salt bridges, based on the high number of basic residues in the AT-Hook 3 peptide.

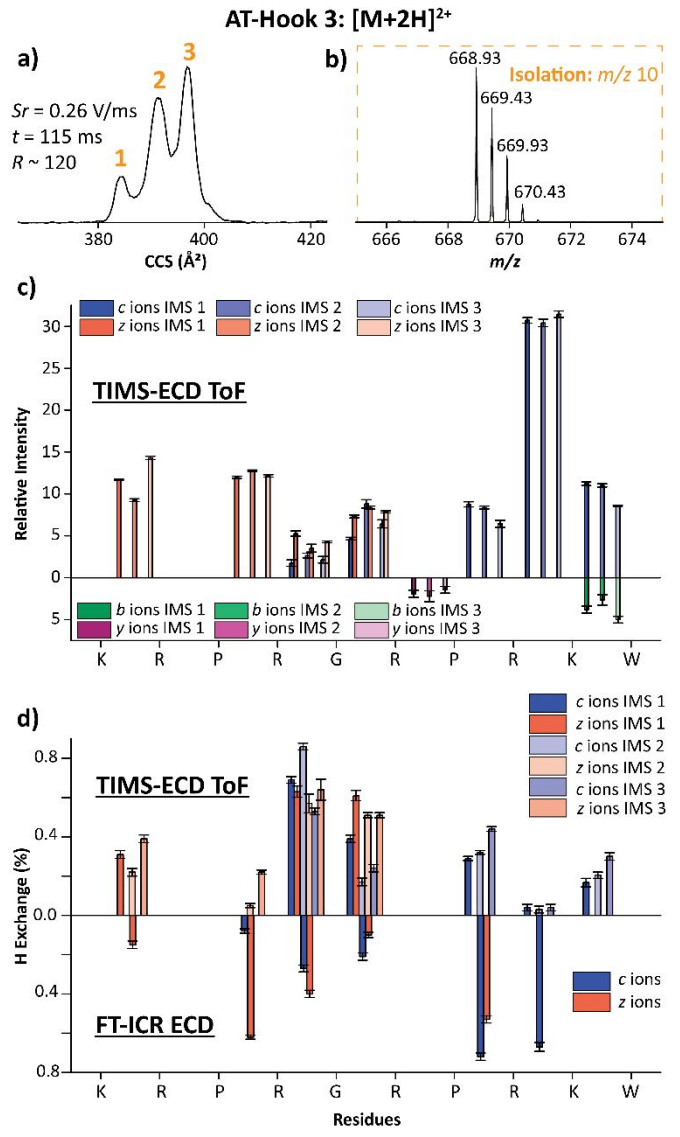

Figure 3. TIMS-q-EMS-ToF and FT-ICR-ECD MS/MS analysis of AT-Hook 3 $[M + 2H]^{2+}$ ions (m/z 555.9). (a) Typical TIMS profiles, (b) quadrupole isolation window of the precursor ion, (c) bar plots showing the relative intensities of the ECD product ions per IMS bands for the selected $[M + 2H]^{2+}$ ions, and (d) bar plot showing the hydrogen migration events of AT-Hook 3 observed in the two MS platforms, obtained by comparison between the experimental and theoretical isotopic patterns. Note that relative intensities were calculated using peak heights and divided by the sum of all fragments for direct comparison across IMS bands. c_i/z_j and b_i/y_j ions are plotted above and below the horizontal axis, respectively in (c). Error bars from triplicate measurements are represented on the bar plots. Ion mobility selected ECD/CID and FT-ICR ECD spectra are shown in Figure S3).

The ion mobility-selected ECD/CID fragmentation patterns (i.e., $c_i'/z_j^{\bullet}$ and b_i/y_j series) of AT-Hook 3 were similar for the three IMS bands, suggesting that these three structures are probably conformers that follow the same protonation scheme. The c_i' series started at c_4' product ions for all IMS selected ECD spectra, suggesting that the Arg4 residue is probably protonated, while the $z_j^{\bullet}$ series started at $z_5^{\bullet}$ fragment ions, suggesting that the Arg6 is also protonated. Note that c_3' product ions were observed in the FT-ICR ECD MS/MS, suggesting that the Arg2 residue could also carry a charge instead of Arg4. These observations are consistent with previous TIMS-MS experiments using single point mutations at Arg residues with a neutral residue (Ala) that established Arg2, Arg4 and/or Arg6 as possible protonated residues.[68] This study also established the *cis*/*trans*-isomerization at Arg2-Pro3 and Arg6-Pro7 peptide bonds.[68]

Differences in the hydrogen migration events were observed across the IMS selected ECD spectra (Figure 3d). One of the differences was observed at the Lys1-Arg2 peptide bond, for which higher H• transfer events (z_9') were observed for IMS 1 and 3 bands as compared to IMS 2 band, suggesting that these residues are in proximity to nearby residues. This is consistent with an Arg2-Pro3 peptide bond in a *cis*-configuration for the IMS 1 and 3 bands, while IMS 2 band probably presents a *trans*-configuration. This feature is also in agreement with lower relative intensity of y_8 product ions for IMS band 1 and 3 as compared to IMS band 2, corresponding to the Arg2-Pro3 peptide bond (purple bars in Figure S3h). The $c_7^{\bullet}$ and $c_9^{\bullet}$ product ions exhibited higher abundances of H• migration for IMS 3 selected ECD spectrum as compared to IMS 1 and 2 selected ECD spectra (Figure 3d). This suggests that the Pro7 residue probably adopts a *cis* configuration for the IMS 3 band, placing the Lys9 and Trp10 residues in proximity to facilitate H• transfer (slower dissociation), in good agreement with lower relative abundances of y_4 product ions (purple bars in Figure S3h). Moreover, IMS 1 and 2 selected ECD spectra presented lower abundances of H• migration events as compared to the IMS 3 band, suggesting a conformational change involving a *trans*-isomerization at Arg6-Pro7 peptide bond which might not be positioned in a way that allows H• transfer as frequently (faster

dissociation) as that observed for the IMS 3 band, also in good agreement with higher relative abundances of y_4 product ions (purple bars in Figure S3h). In summary, the ion mobility-selected ECD fragmentation experiments suggested that the IMS 1-3 bands correspond to *cis*-Pro3/*trans*-Pro7, *trans*-Pro3/*trans*-Pro7 and *cis*-Pro3/*cis*-Pro7, respectively. In addition, abundant H• migration events across the IMS bands were observed at Arg4 and Gly5 residues that may relate to the presence of charge solvation, possibly including salt-bridges, that bring nearby residues in proximity in the Arg4-Gly5 region. Note that the doubly protonated species of angiotensin I (*m/z* 648.9, Figures S4-S5) and bradykinin (*m/z* 530.8, Figures S6-S7) were also investigated using both TIMS-q-EMS-ToF MS/MS and FT-ICR-ECD MS/MS platforms and associated discussion can be found in the supporting information. To further addressed the source of differences in the molecular ion gas-phase structures between the TIMS-q-EMS-ToF MS/MS and the FT-ICR ECD MS/MS, the comparison of the fragmentation spectra with TIMS ON and OFF TIMS-q-EMS-ToF MS/MS showed no differences in the relative intensities (Figure S8). That is, potential ion heating induced during the TIMS separation does not seem to be the source for the differences in the observed patterns; note that TIMS OFF operation is equivalent to that in the FT-ICR MS instrument (ion source orthogonal introduction, dual ion funnel system and pressures).

Conclusions

The analysis of model peptides using online TIMS-q-EMS-ToF MS/MS provided complementary structural information on the intramolecular interactions that stabilize the different gas-phase conformations to those obtained by ion mobility or ECD alone. The potential of this coupling was effectively demonstrated for the doubly protonated molecular ions of four, well studied, model peptides (e.g., substance P, angiotensin I, bradykinin and AT-Hook 3) with heterogeneity in the ion mobility profile. The ion mobility resolving power of the TIMS analyzer allowed for the separation of multiple IMS bands (R ~ 115-145) at short times and then effectively collect ion mobility selected ECD spectra as fast as a 0.2 min experiment time, comparable with those needed for LC pre-separations. Particularly, it was demonstrated that all investigated species were probably conformers, involving *cis*/*trans*-isomerization at X-Pro peptide bond, following the same protonation schemes, in good agreement with previous ion mobility and single point mutation experiments. The ion mobility selected ECD spectra were mainly populated with ECD-like fragments (e.g., $c_i^{'}/z_j^{\bullet}$ series), but CID events (e.g., $b_i^{'}/y_j^{\bullet}$ series) were also observed and their relative abundance varied with the peptide model. The comparison between ion mobility selected ECD spectra and traditional FT-ICR ECD MS/MS spectra showed comparable ECD fragmentation efficiencies but differences in the ratio of radical (•)/prime (') fragment species (H• transfer), which were associated with the differences in detection time after the electron capture event. The capability of performing ion mobility measurements in combination with ECD fragmentations in a lower cost and versatile TIMS-q-EMS-ToF MS/MS platform compared to FT-ICR-ECD MS/MS opens new avenues for wide structural analysis of biomolecules.

Acknowledgements

The authors at FIU acknowledge the financial support from the National Science Foundation Division of Chemistry, under CAREER award CHE-1654274, with co-funding from the Division of Molecular and Cellular Biosciences and from the National Institutes of General Medicine award R01GM134247 to FFL, SBIR awards from the US National Institutes of Health R43GM122131-01 and R44GM122131-02 to VGV. We also thank Dr. Mark E. Ridgeway and Dr. Melvin A Park for helpful discussions during the TIMS-q-EMS-CC-ToF MS/MS development.

References

1 R. A. Zubarev, *Mass Spectrom. Rev.*, 2003, **22**, 57-77.
2 H. J. Cooper, K. Hakansson and A. G. Marshall, *Mass Spectrom. Rev.*, 2005, **24**, 201-222.
3 K. O. Zhurov, L. Fornelli, M. D. Wodrich, U. A. Laskay and Y. O. Tsybin, *Chem. Soc. Rev.*, 2013, **42**, 5014-5030.
4 L. M. Mikesh, B. Ueberheide, A. Chi, J. J. Coon, J. E. Syka, J. Shabanowitz and D. F. Hunt, *Biochim. Biophys. Acta*, 2006, **1764**, 1811-1822.
5 H. Molina, D. M. Horn, N. Tang, S. Mathivanan and A. Pandey, *Proc. Natl. Acad. Sci. USA*, 2007, **104**, 2199-2204.
6 L. Tan, K. L. Durand, X. Ma and Y. Xia, *Analyst*, 2013, **138**, 6759-6765.
7 K. Jeanne Dit Fouque, V. Bisram, J. D. Hegemann, S. Zirah, S. Rebuffat and F. Fernandez-Lima, *Anal. Bioanal. Chem.*, 2019, **411**, 6287-6296.
8 A. Chi, C. Huttenhower, L. Y. Geer, J. J. Coon, J. E. Syka, D. L. Bai, J. Shabanowitz, D. J. Burke, O. G. Troyanskaya and D. F. Hunt, *Proc. Natl. Acad. Sci. USA*, 2007, **104**, 2193-2198.
9 L. Han and C. E. Costello, *J. Am. Soc. Mass Spectrom.*, 2011, **22**, 997-1013.
10 D. T. McLachlin and B. T. Chait, *Curr. Opin. Chem. Biol.*, 2001, **5**, 591-602.
11 H. R. Jung, S. Sidoli, S. Haldbo, R. R. Sprenger, V. Schwammle, D. Pasini, K. Helin and O. N. Jensen, *Anal. Chem.*, 2013, **85**, 8232-8239.
12 N. Siuti, M. J. Roth, C. A. Mizzen, N. L. Kelleher and J. J. Pesavento, *J. Proteome Res.*, 2006, **5**, 233-239.
13 K. Alagesan, H. Hinneburg, P. H. Seeberger, D. V. Silva and D. Kolarich, *Glycoconj. J.*, 2019, **36**, 487-493.
14 Y. Xie, J. Zhang, S. Yin and J. A. Loo, *J. Am. Chem. Soc.*, 2006, **128**, 14432-14433.
15 S. Yin and J. A. Loo, *J. Am. Soc. Mass Spectrom.*, 2010, **21**, 899-907.
16 S. N. Jackson, S. Dutta and A. S. Woods, *J. Am. Soc. Mass Spectrom.*, 2009, **20**, 176-179.
17 H. Zhang, W. Cui, J. Wen, R. E. Blankenship and M. L. Gross, *Anal. Chem.*, 2011, **83**, 5598-5606.
18 R. A. Zubarev, N. L. Kelleher and F. W. McLafferty, *J. Am. Chem. Soc.*, 1998, **120**, 3265-3266.
19 R. A. Zubarev, N. A. Kruger, E. K. Fridriksson, M. A. Lewis, D. M. Horn, B. K. Carpenter and F. W. McLafferty, *J. Am. Chem. Soc.*, 1999, **121**, 2857-2862.
20 J. J. Coon, J. E. P. Syka, J. C. Schwartz, J. Shabanowitz and D. F. Hunt, *Int. J. Mass Spectrom.*, 2004, **236**, 33-42.
21 J. E. Syka, J. J. Coon, M. J. Schroeder, J. Shabanowitz and D. F. Hunt, *Proc. Natl. Acad. Sci. USA*, 2004, **101**, 9528-9533.

22 R. D. Leib, W. A. Donald, M. F. Bush, J. T. O'Brien and E. R. Williams, *J. Am. Soc. Mass Spectrom.*, 2007, **18**, 1217-1231.
23 F. Turecek, *J. Am. Chem. Soc.*, 2003, **125**, 5954-5963.
24 A. Sawicka, P. Skurski, R. R. Hudgins and J. Simons, *J. Phys. Chem. B*, 2003, **107**, 13505-13511.
25 E. A. Syrstad and F. Turecek, *J. Am. Soc. Mass Spectrom.*, 2005, **16**, 208-224.
26 A. Patriksson, C. Adams, F. Kjeldsen, J. Raber, D. van der Spoel and R. A. Zubarev, *Int. J. Mass Spectrom.*, 2006, **248**, 124-135.
27 N. Leymarie, C. E. Costello and P. B. O'Connor, *J. Am. Chem. Soc.*, 2003, **125**, 8949-8958.
28 B. N. Moore, T. Ly and R. R. Julian, *J. Am. Chem. Soc.*, 2011, **133**, 6997-7006.
29 M. D. Wodrich, K. O. Zhurov, A. Vorobyev, H. Ben Hamidane, C. Corminboeuf and Y. O. Tsybin, *J. Phys. Chem. B*, 2012, **116**, 10807-10815.
30 I. Swierszcz, P. Skurski and J. Simons, *J. Phys. Chem. A*, 2012, **116**, 1828-1837.
31 M. M. Savitski, F. Kjeldsen, M. L. Nielsen and R. A. Zubarev, *J. Am. Soc. Mass Spectrom.*, 2007, **18**, 113-120.
32 B. J. Bythell, *J. Phys. Chem. A*, 2013, **117**, 1189-1196.
33 Y. O. Tsybin, H. He, M. R. Emmett, C. L. Hendrickson and A. G. Marshall, *Anal. Chem.*, 2007, **79**, 7596-7602.
34 C. Lin, J. J. Cournoyer and P. B. O'Connor, *J. Am. Soc. Mass Spectrom.*, 2008, **19**, 780-789.
35 K. Jeanne Dit Fouque, H. Lavanant, S. Zirah, J. D. Hegemann, C. D. Fage, M. A. Marahiel, S. Rebuffat and C. Afonso, *Analyst*, 2018, **143**, 1157-1170.
36 M. Perot-Taillandier, S. Zirah, S. Rebuffat, U. Linne, M. A. Marahiel, R. B. Cole, J. C. Tabet and C. Afonso, *Anal. Chem.*, 2012, **84**, 4957-4964.
37 V. G. Voinov, M. L. Deinzer and D. F. Barofsky, *Rapid Commun. Mass Spectrom.*, 2008, **22**, 3087-3088.
38 V. G. Voinov, J. S. Beckman, M. L. Deinzer and D. F. Barofsky, *Rapid Commun. Mass Spectrom.*, 2009, **23**, 3028-3030.
39 V. G. Voinov, M. L. Deinzer and D. F. Barofsky, *Anal. Chem.*, 2009, **81**, 1238-1243.
40 V. G. Voinov, S. E. Bennett, J. S. Beckman and D. F. Barofsky, *J. Am. Soc. Mass Spectrom.*, 2014, **25**, 1730-1738.
41 V. G. Voinov, S. E. Bennett and D. F. Barofsky, *J. Am. Soc. Mass Spectrom.*, 2015, **26**, 752-761.
42 V. G. Voinov, M. L. Deinzer, J. S. Beckman and D. F. Barofsky, *J. Am. Soc. Mass Spectrom.*, 2011, **22**, 607-611.
43 V. G. Voinov, P. D. Hoffman, S. E. Bennett, J. S. Beckman and D. F. Barofsky, *J. Am. Soc. Mass Spectrom.*, 2015, **26**, 2096-2104.
44 J. P. Williams, L. J. Morrison, J. M. Brown, J. S. Beckman, V. G. Voinov and F. Lermyte, *Anal. Chem.*, 2020, **92**, 3674-3681.
45 K. L. Fort, C. N. Cramer, V. G. Voinov, Y. V. Vasil'ev, N. I. Lopez, J. S. Beckman and A. J. R. Heck, *J. Proteome Res.*, 2018, **17**, 926-933.
46 J. B. Shaw, N. Malhan, Y. V. Vasil'ev, N. I. Lopez, A. Makarov, J. S. Beckman and V. G. Voinov, *Anal. Chem.*, 2018, **90**, 10819-10827.
47 J. B. Shaw, W. Liu, Y. V. Vasil Ev, C. C. Bracken, N. Malhan, A. Guthals, J. S. Beckman and V. G. Voinov, *Anal. Chem.*, 2020, **92**, 766-773.
48 M. Zhou, W. Liu and J. B. Shaw, *Anal. Chem.*, 2020, **92**, 1788-1795.
49 Y. Pu, M. E. Ridgeway, R. S. Glaskin, M. A. Park, C. E. Costello and C. Lin, *Anal. Chem.*, 2016, **88**, 3440-3443.
50 P. Massonnet, G. Upert, N. Smargiasso, N. Gilles, L. Quinton and E. De Pauw, *Anal. Chem.*, 2015, **87**, 5240-5246.
51 M. A. Baird and A. A. Shvartsburg, *J. Am. Soc. Mass Spectrom.*, 2016, **27**, 2064-2070.
52 J. L. Campbell, T. Baba, C. Liu, C. S. Lane, J. C. Y. Le Blanc and J. W. Hager, *J. Am. Soc. Mass Spectrom.*, 2017, **28**, 1374-1381.
53 J. Wei, J. Wu, Y. Tang, M. E. Ridgeway, M. A. Park, C. E. Costello, J. Zaia and C. Lin, *Anal. Chem.*, 2019, **91**, 2994-3001.
54 V. V. Gadkari, C. R. Ramirez, D. D. Vallejo, R. T. Kurulugama, J. C. Fjeldsted and B. T. Ruotolo, *Anal. Chem.*, 2020, **92**, 15489-15496.
55 K. Jeanne Dit Fouque, D. Kaplan, V. G. Voinov, F. H. V. Holck, O. N. Jensen and F. Fernandez-Lima, *Anal. Chem.*, 2021.
56 F. A. Fernandez-Lima, D. A. Kaplan, J. Suetering and M. A. Park, *Int. J. Ion Mobil. Spectrom.*, 2011, **14**, 93-98.
57 F. A. Fernandez-Lima, D. A. Kaplan and M. A. Park, *Rev. Sci. Instrum.*, 2011, **82**, 126106.
58 D. R. Hernandez, J. D. Debord, M. E. Ridgeway, D. A. Kaplan, M. A. Park and F. Fernandez-Lima, *Analyst*, 2014, **139**, 1913-1921.
59 M. E. Ridgeway, M. Lubeck, J. Jordens, M. Mann and M. A. Park, *Int. J. Mass Spectrom.*, 2018, **425**, 22-35.
60 K. Michelmann, J. A. Silveira, M. E. Ridgeway and M. A. Park, *J. Am. Soc. Mass Spectrom.*, 2015, **26**, 14-24.
61 J. A. Silveira, K. Michelmann, M. E. Ridgeway and M. A. Park, *J. Am. Soc. Mass Spectrom.*, 2016, **27**, 585-595.
62 M. Chai, M. N. Young, F. C. Liu and C. Bleiholder, *Anal. Chem.*, 2018, **90**, 9040-9047.
63 J. A. Silveira, M. E. Ridgeway and M. A. Park, *Anal. Chem.*, 2014, **86**, 5624-5627.
64 R. S. Glaskin, V. G. Voinov, K. Newton, R. Kurulugama, G. C. Stafford, J. S. Beckman, D. F. Barofsky and C. E. Costello, Presented at the *64th Annual ASMS Conference on Mass Spectrometry and Allied Topics*, San Antonio, TX, June 5-9, 2016.
65 C. R. Conant, D. R. Fuller, Z. Zhang, D. W. Woodall, D. H. Russell and D. E. Clemmer, *J. Am. Soc. Mass Spectrom.*, 2019, **30**, 932-945.
66 D. L. Swaney, G. C. McAlister, M. Wirtala, J. C. Schwartz, J. E. Syka and J. J. Coon, *Anal. Chem.*, 2007, **79**, 477-485.
67 C. R. Conant, D. R. Fuller, T. J. El-Baba, Z. Zhang, D. H. Russell and D. E. Clemmer, *J. Am. Soc. Mass Spectrom.*, 2019, **30**, 919-931.
68 A. Garabedian, A. Bolufer, F. Leng and F. Fernandez-Lima, *Sci. Rep.*, 2018, **8**, 10783.